Electrocatalytic metal hydride generation using concerted proton electron transfer mediators

Authors: Subal Dey[1,2], Fabio Masero[1], Enzo Brack[1], Marc Fontecave[2], Victor Mougel[1]*

Affiliations:

[1]Department of Chemistry and Applied Biosciences, ETH Zürich, Zürich, Switzerland.

[2]Laboratoire de Chimie des Processus Biologiques, UMR 8229 CNRS, Collège de France, Sorbonne Université, Paris, France.

*Corresponding author. Email: mougel@inorg.chem.ethz.ch

Abstract: The electrochemical generation of metal hydride (M-H) species remains one of the major hurdles for a wide range of catalytic reactions to be carried out electrochemically. We introduce here a new strategy for electrocatalytic M-H generation using concerted proton electron transfer (CPET) mediators. We investigate the combination of a series of CPET mediators with the CO_2 electroreduction catalyst [Mn^I(bpy)$(CO)_3$Br] (bpy = 2,2'-bipyridine), probing the reversal of the product selectivity from CO to HCOOH to evaluate the efficiency of the M-H generation step. We demonstrate the formation of the manganese-hydride by *in-situ* spectroscopic techniques and determine the thermodynamic boundary conditions for this mechanism to occur. A synthetic iron-sulfur cluster is identified as the best CPET-mediator for that system, enabling the preparation of a benchmark catalytic system for HCOOH generation.

One-Sentence Summary: An iron-sulfur cluster acts as an efficient mediator to enable electrocatalytic Mn-H generation and subsequent transfer to CO_2.

Main Text:

Transition metal hydrides (M-Hs) are ubiquitous intermediates in a wide number of catalytic reactions, ranging from biological energy conversion to industrial processes. These notably play a central role in the H^+/H_2 interconversion,(*1*) in the reduction of CO_2 to formic acid,(*2*) as well as in a broad range of hydrogenation reactions.(*3, 4*) The facile generation of metal hydrides is arguably one of the most important challenges to address in order to further improve the energy efficiency of these reactions. In particular, the electrochemical generation of M-Hs constitutes one of the main hurdles to overcome to enable the sustainable conversion of small molecules (H_2O, CO_2 and N_2 reduction) using renewable electricity sources.

In mechanistic terms, the electrochemical generation of a M-H typically requires the reduction of the metal center followed by the transfer of a proton and an electron in a stepwise fashion, either via an electron transfer-proton transfer (ET-PT) or a PT-ET sequence (Fig. 1A, grey box).(*5, 6*) Such sequential processes involve the transfer of electrons and protons from different sources (the solid electrode and the electrolyte, respectively) which require the generation of highly reduced oxidation states of the metal center or the use of strong acids, lowering the energy efficiency and rates. Alternatively, the transfer of an electron and a proton can occur in one kinetic step, called concerted proton-electron transfer (CPET). This enables higher rates while requiring only low driving force, *i.e.* moderate reducing potentials and weak acids. In addition, the use of milder proton sources minimizes the chances of quenching the hydride species to generate H_2, a main point to enable high selectivity when H_2 is not the product targeted.

Major advances in M-H mediated electrocatalysis have recently been reported via the introduction of redox mediators to facilitate the ET step(*7, 8*) or via the use of proton shuttles to smoothen the PT step.(*1, 9, 10*) Relatedly, a few examples of electrocatalytic CPET

mediators, capable of the simultaneous transfer of a proton and an electron, have been shown very successful at increasing reaction rates in both oxidative(*11-13*) and reductive processes.(*14, 15*) However, to the best of our knowledge, the use of a CPET mediator to mediate the electrocatalytic generation of a metal hydride has never been reported (Fig. 1A; blue box).

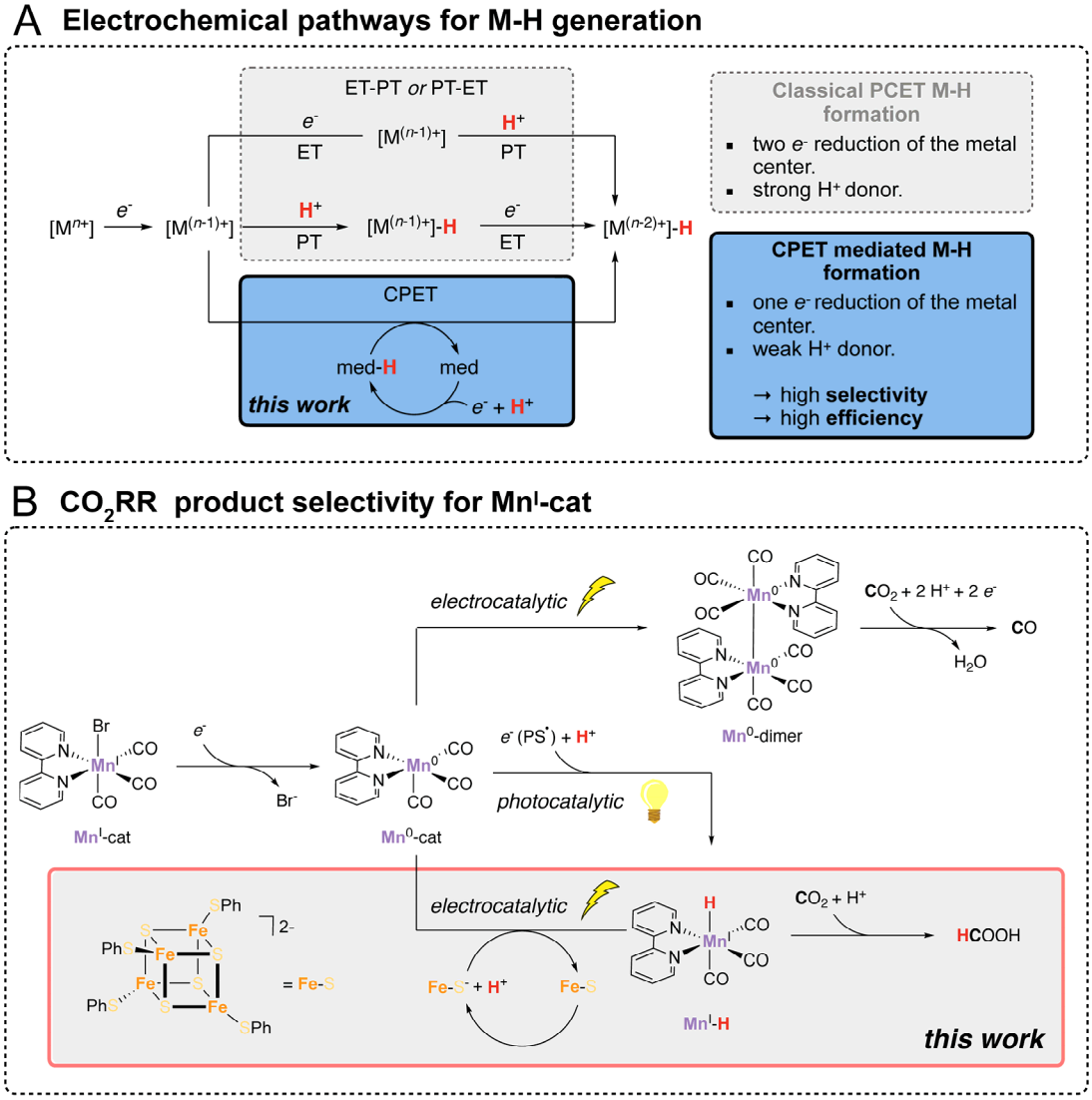

Fig. 1: CPET mediated metal hydride formation (**A**) Generation of M-H species via stepwise electron-proton transfer (ET-PT or PT-ET) and CPET processes. (**B**) Reaction pathways and associated product selectivity for **Mn^{I}-cat** catalyzed CO_2 reduction under electro- and photochemical conditions.

Herein, we demonstrate that the use of appropriately chosen CPET mediators enables the energy efficient electrocatalytic generation of M-H species and explore the potential of this approach for the electrocatalytic transformation of CO_2 (Fig. 1B). We report that the iron-sulfur cluster $[Fe_4S_4(SPh)_4]^{2-}$ (**Fe-S**) can be used as a CPET mediator in presence of $[Mn^{I}(bpy)(CO)_3Br]$ (**Mn^{I}-cat**) to promote the electrocatalytic formation of a manganese hydride species. We demonstrate that this strategy allows shifting the CO_2 reduction reaction (CO_2RR) selectivity of **Mn^{I}-cat** from CO to HCOOH and the identification of one of the most active catalytic systems for the selective reduction of CO_2 to HCOOH. This example enabled us to validate the boundary conditions for the choice of CPET mediators for the electrochemical generation of metal hydrides.

The choice of an appropriate CPET mediator (*med*) for catalytic M-H formation requires optimizing two CPET steps being i.) the (re)generation of the *med*-H species with an electron and a proton (note that *med*-H corresponds here to the mediator *med* that stores one electron and one proton, not necessarily on the same site) and ii.) the overall transfer of an apparent hydrogen atom (*i.e.* a proton and an electron) to the singly reduced metal site (Fig. 1A). The thermodynamic and kinetic parameters to meet for an efficient M-H generation using a CPET mediator are ultimately fixed by the BDFE (bond dissociation free energy) and pK_a values of the generated hydride species, and thus the choice of the CPET mediator used should be tailored to the M-H species targeted and *in fine* to the desired catalytic application. In the present work, we investigated the impact of the proposed CPET-mediated generation of M-Hs in the context of CO_2 electroreduction, as the formation of M-H intermediates is known to impact the catalyst's selectivity and product distribution. Molecular electrocatalysts for CO_2RR are for the vast majority promoting two electron reduction of CO_2 to CO or HCOOH, the latter requiring an M-H intermediate while CO formation typically requires the direct interaction of CO_2 with the metal center and excludes M-H formation.(*2*) Among the widely investigated selective CO_2RR catalysts, we selected **Mn^{I}-cat** thanks to its divergent behavior in the electrochemical and photochemical CO_2RR (Fig. 1B). It produces CO under electrochemical conditions*(16)* while generating HCOOH as the major product in photochemical conditions.(*17*) This change of selectivity relates directly to the reaction pathway involved during catalysis: the C-centered activation of CO_2 under electrochemical conditions leads to CO as the main product while the manganese hydride species (Mn-H) formed under photochemical conditions enables HCOOH formation (Fig. 1B).(*18*) Despite several hypotheses, the factors influencing the formation of Mn-H species in such molecular complexes under photochemical conditions are not fully understood, and recent work highlighted that the proximity of proton donors in the ligand framework may enable the generation of Mn-H species also under electrochemical conditions.(*19, 20*)

An initial screening of the thermodynamic feasibility of such a CPET-mediated Mn-H formation using reported BDFE values(*21, 22*), discussed in further details below in text, motivated our choice of iron-sulfur clusters (Fe-S clusters) as CPET mediators. Synthetic Fe-S clusters have so far never been used to mediate CPET steps in a catalytic context. However, proton-coupled electron transfers mediated by Fe-S clusters have been observed in Fe-Fe hydrogenases (*23*) (H-cluster) as well as in 3Fe-4S cluster containing ferredoxins,(*24*) and recent studies have shown that synthetic Fe-S clusters are also capable of donating or accepting an effective H-atom in a stoichiometric reaction.(*21, 25*) In addition, their very low reorganization energy, which is key to the high efficiency of electron transfers in enzymatic systems,(*26, 27*) is highly desirable for an efficient (re)generation when used as a CPET-mediator. Based on these facts, we investigated the CO_2RR using the synthetic iron-sulfur cluster **Fe-S** as a potential CPET mediator in combination with the well-known CO_2 reduction catalyst **Mn^{I}-cat**.

Under an Ar atmosphere, the cyclic voltammogram (CV) of a 1:1 mixture of both **Mn^{I}-cat** and **Fe-S** cluster in acetonitrile (CH_3CN) (see *Supplementary Materials*, section 2.1.1)) appears identical to the sum of the CVs of its individual components, revealing three consecutive 1 e^- reduction events at -1.34 V, -1.65 V and -2.05 V (Fig. S1; potentials expressed *vs.* Fc/Fc$^+$ here and in all text below). These events were respectively assigned to the **Fe-S**$^{0/-1}$ redox process and to the reduction of **Mn^{I}-cat** to the dimeric complex [Mn^0(bpy)(CO)$_3$]$_2$ (**Mn^0-dimer**) first and the subsequent reduction of the dimer to the **Mn^{-1}-cat** species (Fig. 1B; see *Supplementary Materials*, section 2.1.1 for details).

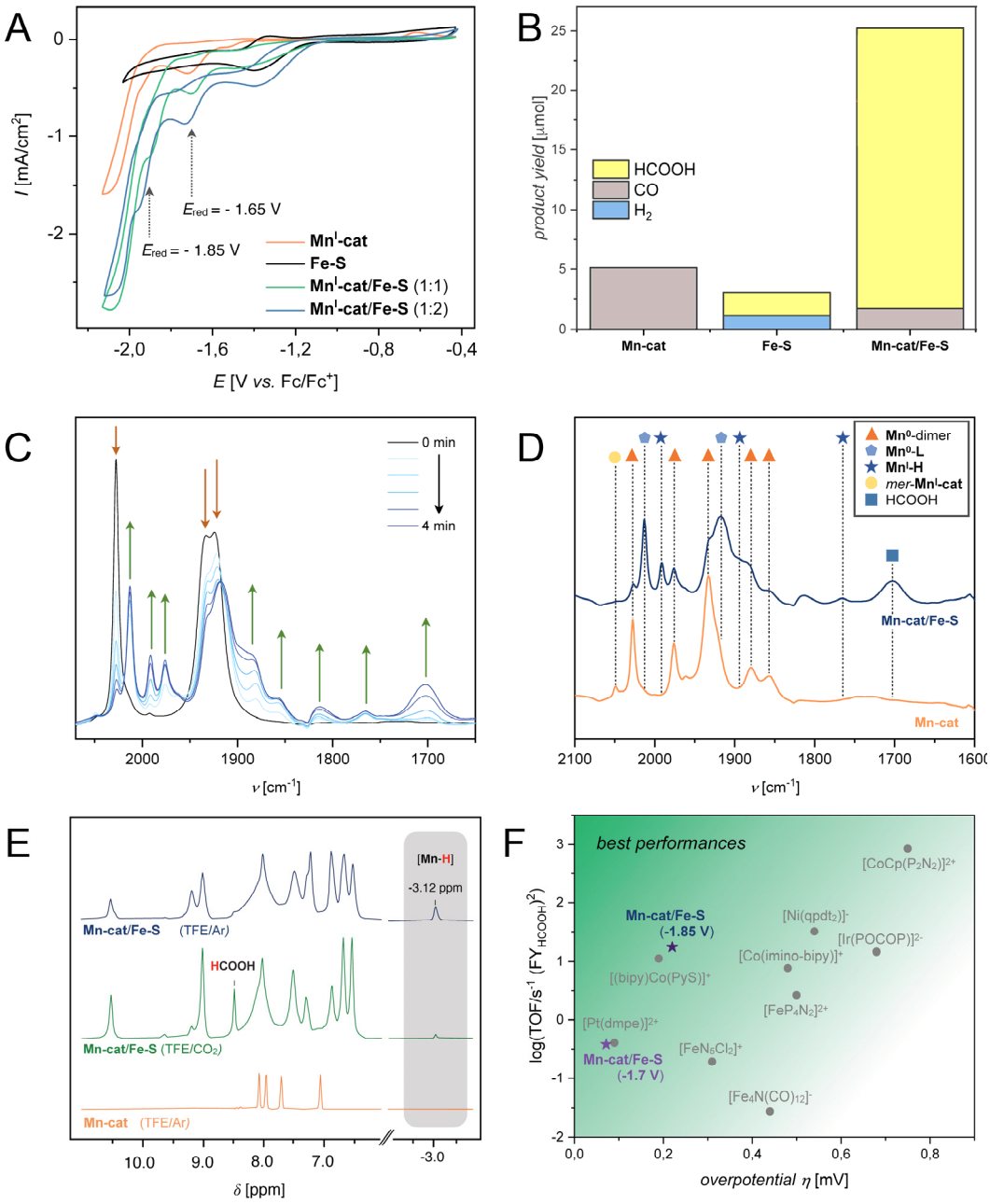

Fig. 2: Catalytic activity and spectroscopic characterization of relevant intermediates of CPET mediated CO_2RR activity of Mn^I-cat. (**A**) Overlaid CV data of **Mn^I-cat** (1 mM) in the absence or in the presence of **Fe-S** along with the CV of **Fe-S** alone in the presence of CO_2 (0.2 M TFE, 0.1 M $TBAPF_6$ in CO_2-saturated CH_3CN). (**B**) Corresponding products obtained during 90 min CPE at -1.85 V using a 1:2 **Mn^I-cat/Fe-S** mixture under identical conditions (0.2 M TFE, 0.1 M $TBAPF_6$ in CO_2-saturated CH_3CN). (**C**) Time dependent evolution of IRSEC signals of a 1:2 **Mn^I-cat/Fe-S** mixture in the presence of CO_2 upon reduction at -1.65 V (40 equiv. TFE, 0.1 M $TBAPF_6$ in CO_2-saturated CH_3CN). (**D**) Overlay of the IRSEC signals after 4 min CPE of a 1:2 **Mn^I-cat/Fe-S** mixture (*blue*) and **Mn^I-cat** only (*red*) under the conditions described in C. (**E**) *Ex-situ* ^{1}H-NMR spectra of **Mn^I-cat** (*orange*) and a 1:1 **Mn^I-cat/Fe-S** mixture recorded after CPE at -1.65 V and addition of 50 equiv. of TFE under Ar (*blue*), and CO_2 (*green*) . (**F**) Comparison of the performance among reported catalytic CO_2RR systems selective for formic acid production (see Table S2 and section 2.8 of the *Supplementary Materials* for details).

This behavior is markedly different under CO_2RR conditions (CO_2-saturated electrolyte solution containing 0.2 M 2,2,2-trifluoroethanol (TFE) as the proton donor, see *Supplementary Materials*, section 2.1.1 for detailed discussion on the choice of experimental conditions and Fig. S1-S6). The CV of the 1:1 mixture of **Mn^I-cat** and **Fe-S** presented in Fig. 2A exhibits two significant changes with respect to the CVs of each complex taken separately: the catalytic current of the peak assigned to the electrochemical CO_2RR activity of **Mn^I-cat** at -2.05 V is enhanced by ca. 50% and a new catalytic feature appears at -1.85 V (note that **Fe-S** alone does not show any catalytic features within the experimental potential range). In addition, a small current enhancement (2.4 times) of the peak at -1.65 V is observed under CO_2RR conditions. In the absence of CO_2 or TFE, the catalytic process at -2.05 V is not present and the process at -1.85 V is substantially lowered, while the **Fe-$S^{0/-1}$** process remained unaltered (Fig. S2 and S3). Increasing the concentration of **Fe-S** (1:2 **Mn^I-cat**/**Fe-S** ratio) does not impact the current of the -2.05 V peak but results in a further increase of the catalytic current at -1.85 V (Fig. 2A). These results suggest that the new catalytic process at -1.85 V is related to the generation of a new catalytic species resulting from the synergistic combination of **Fe-S** and **Mn^I-cat** and occurring at less negative potentials than that required for **Mn^I-cat** alone to reduce CO_2. To identify the reaction catalyzed at this new catalytic process, we carried out a series of 90 min controlled potential electrolyses (CPEs) (Fig. S7). A CPE at-1.85 V revealed a complete shift of product selectivity and formation rates (Fig. 2B): the 1:2 combination of **Mn^I-cat** and **Fe-S** enabled the formation of a large amount of HCOOH with high selectivity (FY_{HCOOH} 92%, n_{HCOOH} = 23 µmol) and a small amount of CO (FY_{CO} 6%, n_{CO} = 1.6 µmol), while **Mn^I-cat** alone catalyzes CO_2RR selectively, as expected, to CO with low activity (FY_{CO} 91%, n_{CO} = 5 µmol) with no formation of H_2 and **Fe-S** alone only produces a very small amount of HCOOH (FY_{HCOOH} 30%, n_{HCOOH} = 1.9 µmol) and H_2 (FY_{H_2} 17%, n_{H_2} = 1 µmol) (Table S1). We identified the 1:2 **Mn^I-cat**/**Fe-S** ratio as optimal, since both the amount of products formed and the selectivity for HCOOH *vs*. CO were enhanced when increasing the concentration of **Fe-S** (*i.e.* decreasing the **Mn^I-cat**/**Fe-S** ratio), reaching a plateau at a 1:2 ratio (Fig. S7 and Table S1). Most importantly, with an overall turnover frequency (TOF) of 20 s^{-1} at an overpotential of only 220 mV measured from the long-term CPE experiment, the 1:2 **Mn-Cat**/**Fe-S** system stands among the best molecular electrocatalytic systems for the reduction of CO_2 to HCOOH, while operating at remarkably high faradaic efficiency (see section 2.8 in *Supplementary Materials* and Fig. 2F). In addition, independently of the selectivity shift, a ca. sixfold increase in turnover number (TON) for CO_2RR was observed with respect to the analogous CPE carried out in the absence of **Fe-S** (Table S1).

Finally, the origin of the above-mentioned increase of the current at -1.65 V under catalytic conditions with the 1:2 **Mn-Cat**/**Fe-S** system was investigated by carrying out a CPE at -1.7 V. Highly selective HCOOH formation was also observed (FY_{HCOOH} 91%, n_{HCOOH} = 9.5 µmol, Table S1) yet with significantly lower rates (TOF = 0.46 s^{-1}) than observed at -1.85 V. Nevertheless, selective reduction of CO_2 to formic acid at such a modest overpotential (70 mV) is to our knowledge unprecedented for 1st row transition metal catalysts (Fig. 2F).

Last, CPE at the third catalytic wave (E_{red} = -2.05 V) with a 1:2 ratio of **Mn^I-Cat**/**Fe-S** revealed an increased CO:HCOOH ratio (FY_{CO} 32%, FY_{HCOOH} 56%) together with small amounts of H_2 (FY_{H_2} 6%). This lowered selectivity for formate is consistent with the combination of the catalytic process at -1.85 V mentioned above and the catalytic process at -2.05 V originating from the residual activity of **Mn^I-Cat**, as suggested by the CV studies. Decomposition of the complexes under catalytic conditions and modulation of the reactivity by potential side-products of the solvolysis of **Fe-S** were ruled out (see *Supplementary Materials*, section 2.9 and Fig. S9 – S10 for detailed discussion).

Such a change of selectivity from CO to HCOOH suggests the formation of a Mn-H intermediate(*19, 20*) in the presence of **Fe-S** and prompted us to investigate reaction intermediates via *in-situ* spectroscopic techniques. *In-situ* infrared spectroscopy (IRSEC) studies under optimized catalytic conditions (CO_2-saturated electrolyte solution, 40 equiv. TFE, 2 mM **Mn^{I}-cat** and 4 mM **Fe-S**), revealed the appearance of the characteristic ν_{CO} vibrations of the Mn(I)-hydride complex [Mn^{I}(bpy)$(CO)_3$H] (**Mn^{I}-H**) at 1990 and 1892 cm^{-1} together with a weak vibration at 1764 cm^{-1} when the potential of the cell was held below ca. -1.65 V. While the carbonyl stretches ν_{CO} of the **Mn^{I}-H** have been reported (Fig. 2C and Fig S11),(*19, 28*) the new 1764 cm^{-1} band observed here lies in the range of reported Mn-H vibrations(*29*) and can be tentatively assigned to the corresponding $\nu_{Mn\text{-}H}$ stretch of **Mn^{I}-H**. None of the vibrations associated to **Mn^{I}-H** are observed in the absence of **Fe-S** or TFE (Fig. S12). With respect to the IRSEC spectrum recorded in the absence of **Fe-S** (Fig. 2D *orange line*), a striking feature of the IRSEC spectrum of the 1:2 **Mn-Cat**/**Fe-S** system (Fig. 2D *blue line*) is the relatively lower intensity of the ν_{CO} vibrations at 1975, 1934, 1878 and 1853 cm^{-1} assigned to **Mn^{0}-dimer** (see Fig. 2D, Table S4 and section 3.1 of *Supplementary Materials*). This suggests that the promoted formation of **Mn^{I}-H** in presence of **Fe-S** hinders the dimerization of the Mn(0) complex [Mn^{0}(bpy)$(CO)_3$] (**Mn^{0}-cat**) to **Mn^{0}-dimer**. In addition, the appearance of a set of ν_{CO} vibrations at 2012, 1935(sh) and 1920 cm^{-1} points to the formation of a neutral [Mn(bpy)$(CO)_3$L] (**Mn^{0}-L**) complex(*28*) (**L** being a neutral ligand such as CH_3CN, Fig. 2D and Fig. S12). Such a complex is not observed in the absence of **Fe-S** and we tentatively attribute its formation to a weak interaction between the reduced cluster $[Fe_4S_4(SPh)_4]^{3-}$ (**Fe-S^{-1}**) and **Mn^{I}-cat** that triggers Br^- release and the subsequent reduction of the cationic acetonitrile complex. *In-situ* formation of HCOOH was further confirmed by the appearance of its characteristic vibration at 1700 cm^{-1}.(*19*) When the potential of the IRSEC cell is shifted slightly further negative (approximatively -1.85 V), we observed a decay of the vibrations associated to **Mn^{I}-H** along with the growth of at the vibration 1700 cm^{-1} suggesting intense formic acid generation (Fig. S14). The additional vibrations at 1911 and 1810 cm^{-1}, which further grow when the potential of the cell is shifted to more negative values are attributed to [Mn(bpy)$(CO)_3$]$^-$ (**Mn^{-1}-cat**).(*30*) **Mn^{-1}-cat** catalyzes the selective reduction of CO_2 to CO and its gradual appearance at the most negative potentials is consistent with the increased FYs for CO observed in CPE experiments at potentials below -1.85 V.

Formation of **Mn^{I}-H** was further confirmed by the appearance of a hydride resonance at -3.12 ppm in the ^{1}H NMR of a 1:1 solution of **Mn-Cat**/**Fe-S**, reduced by a CPE step at -1.65 V in CD_3CN followed by the addition of a CO_2 saturated TFE/CD_3CN solution (2 M, 30 µL) to the NMR tube (Fig. 2E, *green* spectrum). The simultaneous appearance of a HCOOH peak (δ = 8.4 ppm) in the ^{1}H NMR spectrum confirms the catalytic activity of the complex at that potential and explains the low intensity of the **Mn^{I}-H** signal, as it is consumed to generate HCOOH. Consequently, the appearance of the hydride resonance is even more pronounced when the same experiment is carried out in the absence of CO_2 (Fig. 2E, *blue* spectrum. None of the signals associated with **Mn^{I}-H** were observed in the absence of **Fe-S** under identical condition (Fig. 2E, *yellow* spectrum, the ^{1}H NMR confirming instead the formation of **Mn^{0}-dimer** observed in IRSEC experiments (See section 4 of the *Supplementary Materials* for details).

Taken together with the CV data presented above, the IRSEC and ^{1}H NMR data provide evidence for the formation of **Mn^{I}-H**. **Mn^{I}-H** generation is observed after the 1 e^- reduction of **Mn^{I}-cat** to **Mn^{0}-cat**, which occurs at a potential where **Fe-S** is already in the reduced **Fe-S^{-1}** form. Nonetheless, the absence of any IR features for **Mn^{-1}-cat** at this potential when no proton source was added (Fig. S12) rules out the possibility of an ET-PT mechanism mediated by **Fe-S** and generating **Mn^{I}-H** upon protonation of **Mn^{-1}-cat**. Relatedly, the

quantitative dimerization of **Mn^0-cat** observed in the absence of **Fe-S** at the potentials required for **Mn^I-H** formation (Fig. S12), excludes a PT-ET mechanism. This is consistent with a CPET from an *in situ* generated [**Fe-S**]**H** species to **Mn^0-cat** to generate **Mn^I-H**. It highlights that the ability of iron-sulfur clusters to promote CPET, known for stoichiometric reactions,(*21*) can be exploited in a catalytic pathway. Most importantly, **Fe-S** acts as a CPET mediator for the catalytic generation of a manganese hydride species.

This prompted us to attempt determining the thermodynamic and kinetic feasibility of such a CPET-mediated metal hydride generation. As mentioned above, two CPET steps have to be considered, being i.) the (re)generation of the *med*-H species with an electron and a proton and ii.) the overall transfer of an apparent hydrogen atom to the singly reduced metal site [$M^{(n-1)+}$] (Fig. 3A). Both steps can be interpreted in a Marcus-type formalism where the proton and electron is treated quantum mechanically and tunnel to the product state through the same transition state while the solvent and other reactants are treated classically. By analogy with the Marcus expression of a single charge transfer, the free-energy barrier and Arrhenius rate constant for a weakly coupled non-adiabatic CPET can be expressed according to the following expression:(*31*)

$$\Delta G^{\ddagger}_{\mathrm{CPET}} = \frac{(\Delta G^{\circ}_{CPET} + \lambda)^2}{4\lambda} \qquad (1)$$

$$k_{\mathrm{CPET}} = A\, e^{\left(\frac{-\Delta G^{\ddagger}_{\mathrm{CPET}}}{k_{\mathrm{B}}T}\right)} = A\, e^{\left(\frac{-(\Delta G^{\circ}_{\mathrm{CPET}} + \lambda)^2}{4\lambda k_{\mathrm{B}}T}\right)} \qquad (2)$$

, where k_{CPET} is the rate, $\Delta G^{\circ}_{\mathrm{CPET}}$ the standard free energy, $\Delta G^{\ddagger}_{\mathrm{CPET}}$ the activation barrier and λ the reorganization energy of the CPET process. A is the pre-exponential factor that is determined from the overlap integrals of the electronic states and proton vibrational states between the substrate and product. T is the absolute temperature and k_{B} is the Boltzmann constant.

In such an approach, a symmetric dependence between the rate of the reaction (k_{CPET}) and the thermodynamic driving force ($\Delta G^{\circ}_{\mathrm{CPET}}$) is expected, resulting in a lower activation barrier than required for the stepwise ET-PT and PT-ET processes. This dependence may be diminished by the fact that both a proton and an electron must synchronously tunnel, resulting in a potentially higher pre-exponential factor (A) than for isolated ET and PT steps. Nevertheless, the use of mild reducing agents and weak acid sources should mitigate that fact and enable faster CPET rates, while being highly beneficial for catalytic purposes since proceeding at a lower overall driving force $\Delta G^{\circ}_{\mathrm{CPET}}$. Hence, considering the two steps of a catalytic CPET generation of a M-H species in the Marcus formalism as presented in Fig. 3 allows identifying boundary conditions for an effective catalytic M-H formation, occurring at high rate and minimal thermodynamic cost.

First, the efficient (re)generation of the CPET mediator requires to minimize the driving force ΔG°_1 and the reorganization energy λ_1 for the generation step *med* → *med*-H. ΔG°_1 corresponds to the BDFE of the *med*-H species, and can be estimated using the Bordwell equation (3):

$$\mathrm{BDFE} = 1.346 \times \mathrm{p}K_{\mathrm{a}} + 23.06 \times E^0 + C_{\mathrm{G}} \qquad (3)$$

, using as E^0 the reduction potential of the $med^{0/-}$ couple and as pK_{a} the value for *med*-H The two main parameters impacting the reorganization energy λ_1 are the solvent reorganization energy and the inner-sphere reorganization energy of the mediator, related to the intrinsic geometry change that occurs upon generation of the *med*-H species. In the specific case of a CPET mechanism, the overall charge will not vary, and the main contributor to the overall reorganization energy will be the inner-sphere ones. A good strategy to lower λ_1 is hence to select a mediator with minimal structural and polarity changes upon CPET.

Second, from a thermodynamic point of view, for the CPET transfer to occur from *med*-H to the reduced metal complex M (*i.e.* $\Delta G^{\circ}_2 < 0$), the BDFE of the *med*-H species ($BDFE^{med\text{-}H}$) should be lower than the BDFE of the corresponding M-H species ($BDFE^{M\text{-}H}$) formed.(*32*) These values should yet be close to lower the associated kinetic energy barrier, as highlighted above.

Last, to ensure an efficient proton transfer from the proton source to the mediator, a proton source fulfilling the relation $pK_a^{proton\ source} \leq pK_a^{med\text{-}H}$ should be selected. Additional selection factors come into play when H_2 generation is not the reaction of interest and will be discussed below in the text.

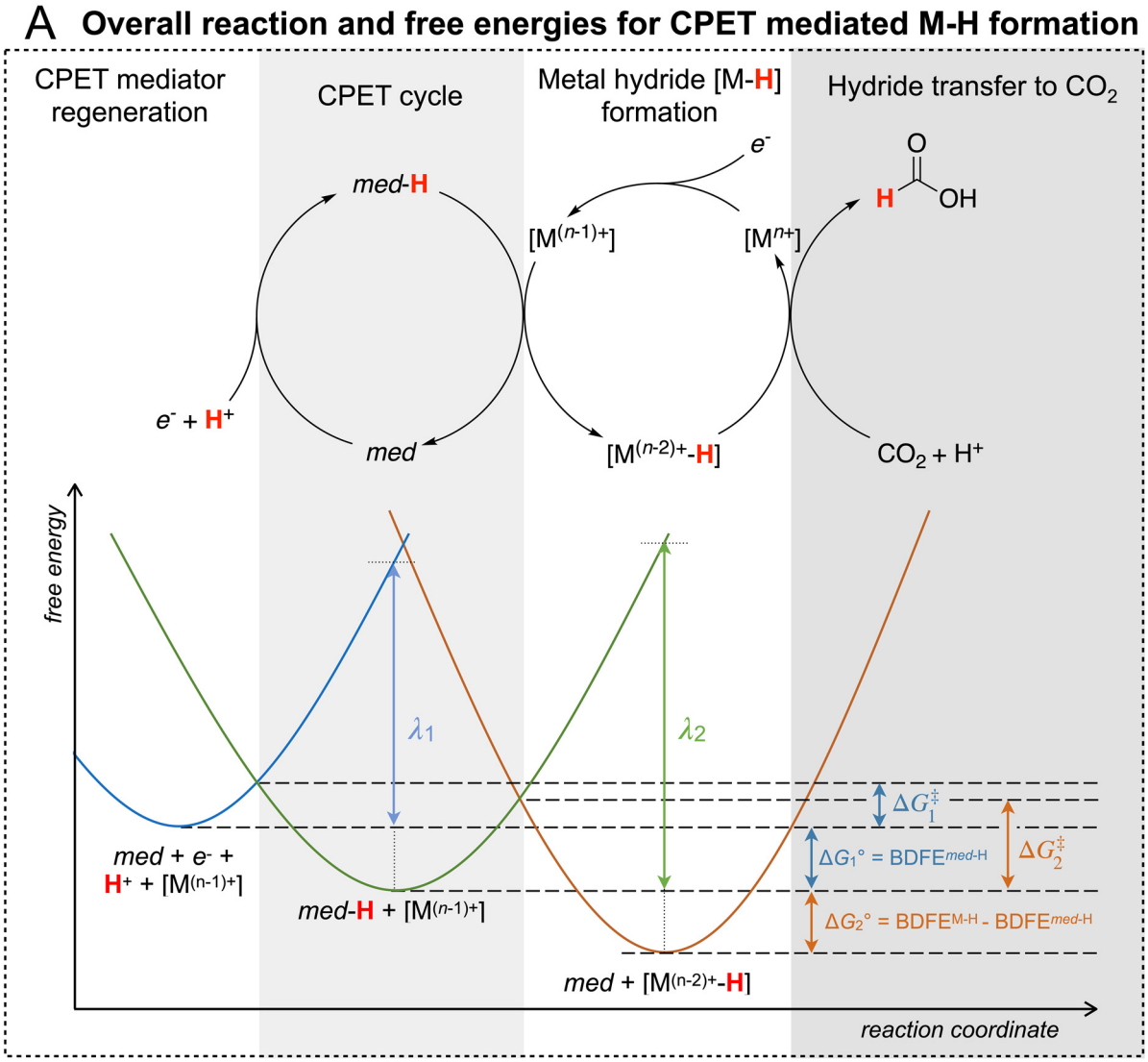

Fig. 3: Thermodynamic and kinetic considerations for catalytic CPET mediated metal hydride formation. (**A**) Schematic representation of the reaction steps in a CPET mediated M-H generation followed by hydride transfer to CO_2 and the associated free-energy parabola representation. (**B**) Boundary conditions to be met to ensure catalytic CPET-mediated M-H generation.

Hence, for the present system, an effective CPET can occur if the $BDFE^{[Fe\text{-}S]H}$ is lower than that of $BDFE^{Mn\text{-}H}$. However, verifying this condition first implies determining these BDFEs that were not previously reported. We determined $BDFE^{[Fe\text{-}S]H}$ here as low as 63.5 kcal/mol using the Bordwell equation (3), in good agreement with the BDFE value of 60.5 kcal/mol (approx.) recently reported for another Fe-S cluster bearing substituted thioaryloxide ligands.(*21*) The determination of this value necessitated evaluating the pK_a value of **[Fe-S]H**, which we determined electrochemically using a protonated P1 phosphazene base (see in *Supplementary Materials*, section 5) and found a value of 30.3 ± 0.3. This value lies in the expected range for this species assuming that a one electron transfer increases the pK_a by 4-6 units compared to the oxidized species as observed for synthetic Fe_2S_2 clusters.(*25*) The lower limit of $BDFE^{Mn\text{-}H}$ was estimated to 65.8 kcal/mol on the basis of CV and ^{1}H NMR data (see in the *Supplementary Materials*, section 6). This value is slightly higher than those reported for other manganese hydride complexes such as $HMn(CO)_5$ (60 kcal/mol) and $HMn(CO)_4PPh_3$ (61 kcal/mol).(*22*) In order to further assess and confirm the lower limit of the BDFE value for **Mn^I-H**, we studied the CO_2 electroreduction activity and respective product ratio between CO and HCOOH of **Mn^I-cat** in the presence of a series of CPET mediators (Fig. 4A) covering a range of BDFE values around this estimated lower boundary. This strategy enables the indirect evaluation of $BDFE^{Mn\text{-}H}$: The presence of significant amounts of HCOOH as a reaction product reveals the formation of **Mn^I-H**, and indicates that the $BDFE^{Mn\text{-}H}$ is lower than the BDFE of the mediator to provide the upper boundary value for $BDFE^{Mn\text{-}H}$, while its absence indicates that **Mn^I-H** is not generated and provides a lower boundary value for $BDFE^{Mn\text{-}H}$. As **Mn^I-H** is formed in the presence of **Fe-S**, we focused our study on CPET mediators that are reported to have BDFE values close to or larger than $BDFE^{[Fe\text{-}S]H}$ mentioned above. Fig. 4B reveals that the amount of HCOOH is lowered with increasing the $BDFE^{med\text{-}H}$ of the CPET mediator using $[Ru^{II}(acac)_2(PyImz)]$ (**Ru-NH**) (acac = acetylacetonate, PyImz = 2-pyridyl-imidazole) and 2,5-di-*tert*-butylhydroquinone (**DTH_2Q**) and finally vanished in the presence of 1,4-dihydroquinone (**H_2Q**) or phenol (**PhOH**) where CO was observed to be the sole CO_2RR product (see *Supplementary Materials*, section 7 for details). The reported BDFE values of this series of CPET donors allow concluding that the generation of **Mn^I-H** occurs in presence of CPET donors with $BDFE^{med\text{-}H}$ below 63.5 kcal/mol but not in presence of CPET donors with $BDFE^{med\text{-}H}$ higher than 67.3 kcal/mol. This suggests that $BDFE^{Mn\text{-}H}$ for **Mn^I-H** lies in between these two values, in good agreement with the experimentally determined lower boundary of 65.8 kcal/mol. This first evaluation of the $BDFE^{Mn\text{-}H}$ of **Mn^I-H** allows determining the thermodynamic feasibility of the hydride transfer from **Mn^I-H** to CO_2 from a hydricity point of view.(*33, 34*) The lower limit of hydricity of the **Mn^I-H** is estimated to ca. 54.4 kcal/mol according to the standard reduction potential correlation (see *Supplementary Materials*, section 8). This is significantly higher than the thermodynamic threshold for HCOOH production (44 kcal/mol),(*34*) in agreement with the sluggish HCOOH generation mentioned above when CPE is carried out at -1.7 V and confirms that **Mn^I-H** needs to be further reduced to generate the more active catalyst. This reduction occurs at ca. -1.85 V to generate a formal **Mn^0-H** species, whose BDFE value can be approximated ca. 10-15 kcal/mol lower than that of **Mn^I-H**.(*35, 36*) The hydricity value of **Mn^0-H** is hence fully consistent with the observed high selectivity and faster rate for HCOOH production. This later finding permits to validate the reaction pathway for the fast electrocatalytic CO_2RR to formic acid by the composite system (**Mn^I-cat/Fe-S**) shown in Fig. 4D: **Fe-S** mediates a CPET step to electrogenerated **Mn^0-cat** affording **Mn^I-H** while hindering the competitive dimerization of **Mn^0-cat**; **Mn^I-H** is further reduced to generate **Mn^0-H** that subsequently mediates a hydride transfer to CO_2 to generate formic acid.

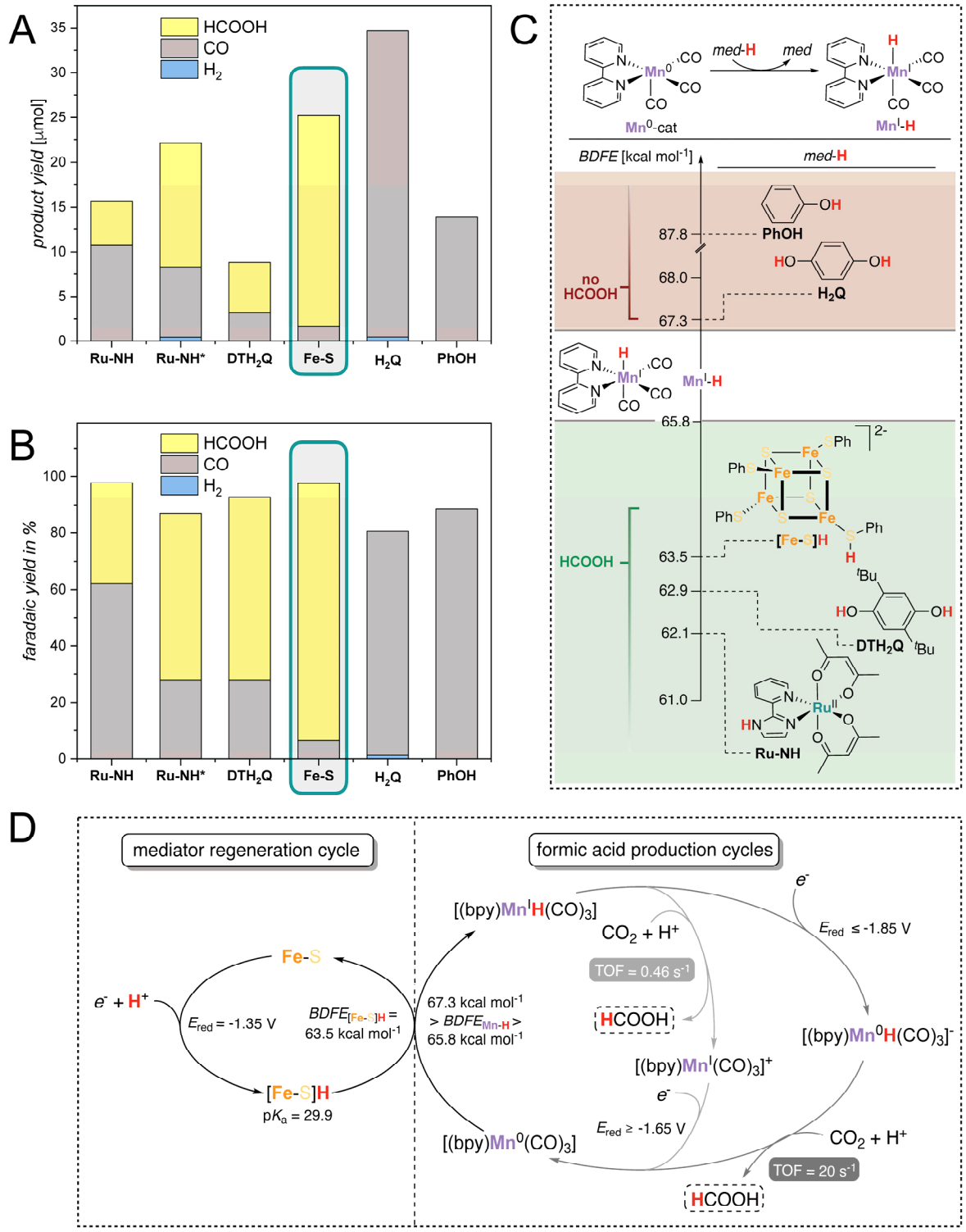

Fig. 4: CO_2RR activity of Mn^I-cat in presence of various CPET mediators: (**A**) Product yields and (**B**) associated faradaic efficiencies for CO_2RR using **Mn^I-cat** in presence of various CPET mediators. The first three entries from the left correspond to experiments carried out in presence of proton source (0.2 M TFE except for **Ru-NH*** where 1.5 M H_2O was used) while the other entries relate to catalytic tests carried out in the absence of proton source and at high concentration of the CPET mediator (0.1-0.5 M). (**C**) Scaling relation of $BDFE^{med\text{-}H}$ with formic acid production, that lead to the determination of $BDFE^{Mn\text{-}H}$ via the reaction shown on *top*. The BDFE values mentioned here are summarized in section 6 of

Supplementary Materials. (**D**) Proposed mechanistic cycle for **Fe-S** mediated **Mn^{I}-H** formation and subsequent transfer of the hydride to CO_2.

The determined BDFE and hydricity values also provide an insight on the observed reverse selectivity towards formic acid generation when **Mn^{I}-cat** is used for photochemical CO_2RR. The typical observed decrease of the BDFE for the composite system made of the photosensitizer and the proton source to values below 40 kcal/mol upon light excitation(*37*) is sufficient to trigger the formation of **Mn^{I}-H** and formic acid production.

In addition, these electrocatalytic tests in presence of various CPET mediators highlight several key features regarding the role of these mediators on the catalytic activity of **Mn^{I}-cat**. First, a substantial enhancement of CO_2RR activity of **Mn^{I}-cat** was observed also in presence of CPET mediators such as **H_2Q** without change of selectivity (Fig2B and Fig 4A), promoting the selective CO_2RR to CO. We assigned this strong rate enhancement to the fact that the BDFE value of **H_2Q** is too high to enable the generation of **Mn^{I}-H** species, but that **H_2Q** still acts as a CPET mediator to enhance the rate of CO_2 reduction, promoting faster proton-electron transfer to the activated CO_2 molecule in the known CO_2 to CO reaction pathway using **Mn^{I}-cat**.(*38*) Such rate enhancement without a change in selectivity has recently been reported for CO_2RR to CO using iron porphyrin complexes in combination with a synthetic NADH analogue as CPET mediator.(*39*) Second, the CO_2RR catalytic performances for HCOOH obtained using **Fe-S** as mediator (TON_{HCOOH} =~4) are significantly better than using **Ru-NH** (TON_{HCOOH} =~0.8) and **DTH_2Q** (TON_{HCOOH} =~0.9) (Table S1). .

The small difference in BDFE values of the above mentioned CPET mediators (below 1 kcal/mol between **Ru-NH**, **DTH_2Q** and **Fe-S**) appears unlikely to explain this strong discrepancy in CO_2RR TONs for HCOOH. We hypothesized that the lower observed TONs resulted from the two points identified above as critical for an efficient regeneration of the CPET mediators, namely the ability of the proton source to transfer a proton to the mediator and the fast reduction of the oxidized mediator. **Ru-NH** here fails at meeting the first point, as the low pK_a of **Ru-NH** (pK_a = 22) significantly hinders the protonation of the corresponding base (**Ru-N^-**) in the presence of TFE under a CO_2 atmosphere (pK_a = 25.1). To confirm this hypothesis, we carried out an analogous CPE experiment using **Ru-NH** as a mediator but in presence of 1.5 M H_2O instead of TFE. In such conditions, the *in situ* generated H_2CO_3 (pK_a = 17 in CH_3CN) should enable the protonation of the electrogenerated **Ru-N^-** species. CPE data confirmed this hypothesis with an enhancement in TON (2.3) and FY for HCOOH production (60%). However, the presence of H_2 suggests that protonation of the Mn hydride species occurs in presence of stronger acid and further illustrates the importance of avoiding the use of proton sources with lower pK_a values. Similarly, we hypothesize the pK_a value of **DTH_2Q** is too low to enable its regeneration in the reaction conditions even using H_2O instead of TFE (see section 7 of *Supplementary Materials*). To mitigate that point, we carried out a CPE in presence of a large excess of **DTH_2Q** (0.11 M) and no TFE, and observed substantially higher FY for HCOOH (65%) and a lower amount of CO (FY = 28%), highlighting the ability of **DTH_2Q** to quantitively generate **Mn^{I}-H**. Nevertheless, the reaction rates remained slow and the TON moderate (Fig. S16 and Table S5). We conjectured that the lower performance of **DTH_2Q** results from kinetic limitations arising from its high steric bulk, that in a Marcus normal region can be translated into an increased donor-acceptor distance lowering both rates for CPET transfer and regeneration at the electrode.

These results further highlight that **Fe-S** is a remarkably effective CPET mediator for the current catalytic system, as it perfectly fulfills the boundary conditions described in Fig. 3A:

it possesses a low $BDFE^{[Fe\text{-}S]H}$, verifies the $BDFE^{[Fe\text{-}S]H} < BDFE^{Mn\text{-}H}$ relationship and can be efficiently regenerated by protonation of the reduced **Fe-S**$^-$ species with TFE, as its pK_a value is significantly higher than the pK_a value of TFE under a CO_2 atmosphere (25.1). In addition, the close BDFE values of **[Fe-S]H** and **Mn^I-H** and the intrinsic low reorganization energy of **Fe-S** allow maximizing the efficiency of the (re)generation of the CPET mediator. Relatedly, this efficient regeneration in presence of mild proton sources prevents the direct protonation of the Mn hydride species generated upon CPET and ensures a high selectivity towards undesired H_2 evolution.

These results serve as a proof of concept for the rational choice of a CPET mediator enabling catalytic metal hydride formation and showcase the potential of synthetic Fe-S clusters as CPET mediators owing to their low reorganization energy, the simple tuning of their redox potential upon modulation of their ligand framework. A wide number of catalytic reactions for which metal hydrides have been identified as key intermediates could benefit from the approach and guiding principle presented in this work.

References and Notes

1. R. M. Bullock, M. L. Helm, Molecular Electrocatalysts for Oxidation of Hydrogen Using Earth-Abundant Metals: Shoving Protons Around with Proton Relays. *Acc. Chem. Res.* **48**, 2017-2026 (2015).
2. R. Francke, B. Schille, M. Roemelt, Homogeneously Catalyzed Electroreduction of Carbon Dioxide—Methods, Mechanisms, and Catalysts. *Chem. Rev.* **118**, 4631-4701 (2018).
3. D. Wang, D. Astruc, The Golden Age of Transfer Hydrogenation. *Chem. Rev.* **115**, 6621-6686 (2015).
4. C. Gunanathan, D. Milstein, Applications of Acceptorless Dehydrogenation and Related Transformations in Chemical Synthesis. *Science* **341**, 1229712 (2013).
5. N. Elgrishi, D. A. Kurtz, J. L. Dempsey, Reaction Parameters Influencing Cobalt Hydride Formation Kinetics: Implications for Benchmarking H_2-Evolution Catalysts. *J. Am. Chem. Soc.* **139**, 239-244 (2017).
6. T. Huang, E. S. Rountree, A. P. Traywick, M. Bayoumi, J. L. Dempsey, Switching between Stepwise and Concerted Proton-Coupled Electron Transfer Pathways in Tungsten Hydride Activation. *J. Am. Chem. Soc.* **140**, 14655-14669 (2018).
7. H. Noh *et al.*, Redox-Mediator-Assisted Electrocatalytic Hydrogen Evolution from Water by a Molybdenum Sulfide-Functionalized Metal–Organic Framework. *ACS Catal.* **8**, 9848-9858 (2018).
8. B. Rausch, M. D. Symes, L. Cronin, A Bio-Inspired, Small Molecule Electron-Coupled-Proton Buffer for Decoupling the Half-Reactions of Electrolytic Water Splitting. *J. Am. Chem. Soc.* **135**, 13656-13659 (2013).
9. A. Dutta, A. M. Appel, W. J. Shaw, Designing electrochemically reversible H_2 oxidation and production catalysts. *Nat. Rev. Chem.* **2**, 244-252 (2018).
10. N. E. Smith, W. H. Bernskoetter, N. Hazari, The Role of Proton Shuttles in the Reversible Activation of Hydrogen via Metal–Ligand Cooperation. *J. Am. Chem. Soc.* **141**, 17350-17360 (2019).
11. A. Badalyan, S. S. Stahl, Cooperative electrocatalytic alcohol oxidation with electron-proton-transfer mediators. *Nature* **535**, 406-410 (2016).
12. E. A. McLoughlin, K. C. Armstrong, R. M. Waymouth, Electrochemically Regenerable Hydrogen Atom Acceptors: Mediators in Electrocatalytic Alcohol Oxidation Reactions. *ACS Catal.* **10**, 11654-11662 (2020).

13. C. M. Galvin, R. M. Waymouth, Electron-Rich Phenoxyl Mediators Improve Thermodynamic Performance of Electrocatalytic Alcohol Oxidation with an Iridium Pincer Complex. *J. Am. Chem. Soc.* **142**, 19368-19378 (2020).
14. M. J. Chalkley, P. Garrido-Barros, J. C. Peters, A molecular mediator for reductive concerted proton-electron transfers via electrocatalysis. *Science* **369**, 850 (2020).
15. C. W. Anson, S. S. Stahl, Cooperative Electrocatalytic O_2 Reduction Involving Co(salophen) with p-Hydroquinone as an Electron–Proton Transfer Mediator. *J. Am. Chem. Soc.* **139**, 18472-18475 (2017).
16. M. Bourrez, F. Molton, S. Chardon-Noblat, A. Deronzier, [Mn(bipyridyl)$(CO)_3$Br]: an abundant metal carbonyl complex as efficient electrocatalyst for CO_2 reduction. *Angew. Chem. Int. Ed.* **50**, 9903-9906 (2011).
17. H. Takeda, H. Koizumi, K. Okamoto, O. Ishitani, Photocatalytic CO_2 reduction using a Mn complex as a catalyst. *Chem. Commun.* **50**, 1491-1493 (2014).
18. X. Wang *et al.*, Site-isolated manganese carbonyl on bipyridine-functionalities of periodic mesoporous organosilicas: efficient CO_2 photoreduction and detection of key reaction intermediates. *Chem. Sci.* **8**, 8204-8213 (2017).
19. M. H. Rønne *et al.*, Ligand-Controlled Product Selectivity in Electrochemical Carbon Dioxide Reduction Using Manganese Bipyridine Catalysts. *J. Am. Chem. Soc.* **142**, 4265-4275 (2020).
20. M. Bhattacharya, S. Sebghati, R. T. VanderLinden, C. T. Saouma, Toward Combined Carbon Capture and Recycling: Addition of an Amine Alters Product Selectivity from CO to Formic Acid in Manganese Catalyzed Reduction of CO_2. *J. Am. Chem. Soc.* **142**, 17589-17597 (2020).
21. C. T. Saouma, W. D. Morris, J. W. Darcy, J. M. Mayer, Protonation and Proton-Coupled Electron Transfer at S-Ligated [4Fe-4S] Clusters. *Chem. Eur. J.* **21**, 9256-9260 (2015).
22. M. Tilset, V. D. Parker, Solution homolytic bond dissociation energies of organotransition-metal hydrides. *J. Am. Chem. Soc.* **111**, 6711-6717 (1989).
23. M. Senger *et al.*, Proton-Coupled Reduction of the Catalytic [4Fe-4S] Cluster in [FeFe]-Hydrogenases. *Angew. Chem. Int. Ed.* **56**, 16503-16506 (2017).
24. R. Camba *et al.*, Mechanisms of Redox-Coupled Proton Transfer in Proteins: Role of the Proximal Proline in Reactions of the [3Fe-4S] Cluster in Azotobacter vinelandii Ferredoxin I. *Biochemistry* **42**, 10589-10599 (2003).
25. A. Albers *et al.*, Fast Proton-Coupled Electron Transfer Observed for a High-Fidelity Structural and Functional [2Fe–2S] Rieske Model. *J. Am. Chem. Soc.* **136**, 3946-3954 (2014).
26. P. Kennepohl, E. I. Solomon, Electronic Structure Contributions to Electron-Transfer Reactivity in Iron−Sulfur Active Sites: 3. Kinetics of Electron Transfer. *Inorg. Chem.* **42**, 696-708 (2003).
27. E. Sigfridsson, M. H. M. Olsson, U. Ryde, Inner-Sphere Reorganization Energy of Iron−Sulfur Clusters Studied with Theoretical Methods. *Inorg. Chem.* **40**, 2509-2519 (2001).
28. F. Franco *et al.*, Local Proton Source in Electrocatalytic CO_2 Reduction with [Mn(bpy–R)$(CO)_3$Br] Complexes. *Chem. Eur. J.* **23**, 4782-4793 (2017).
29. F. A. Cotton, J. L. Down, G. Wilkinson, 167. Infrared spectra of manganese carbonyl hydride and deuteride. *J. Chem. Soc.*, 833-837 (1959).
30. C. W. Machan, M. D. Sampson, S. A. Chabolla, T. Dang, C. P. Kubiak, Developing a Mechanistic Understanding of Molecular Electrocatalysts for CO_2 Reduction using Infrared Spectroelectrochemistry. *Organometallics* **33**, 4550-4559 (2014).
31. S. Hammes-Schiffer, Theoretical Perspectives on Proton-Coupled Electron Transfer Reactions. *Acc. Chem. Res.* **34**, 273-281 (2001).

32. J. M. Mayer, Understanding Hydrogen Atom Transfer: From Bond Strengths to Marcus Theory. *Acc. Chem. Res.* **44**, 36-46 (2011).
33. K. M. Waldie, A. L. Ostericher, M. H. Reineke, A. F. Sasayama, C. P. Kubiak, Hydricity of Transition-Metal Hydrides: Thermodynamic Considerations for CO_2 Reduction. *ACS Catal.* **8**, 1313-1324 (2018).
34. B. M. Ceballos, J. Y. Yang, Directing the reactivity of metal hydrides for selective CO_2 reduction. *Proc. Nat. Acad. Sci.* **115**, 12686 (2018).
35. T. H. Parsell, M.-Y. Yang, A. S. Borovik, C−H Bond Cleavage with Reductants: Re-Investigating the Reactivity of Monomeric $Mn^{III/IV}$−Oxo Complexes and the Role of Oxo Ligand Basicity. *J. Am. Chem. Soc.* **131**, 2762-2763 (2009).
36. S. Pattanayak *et al.*, Spectroscopic and Reactivity Comparisons of a Pair of bTAML Complexes with Fe^{V}═O and Fe^{IV}═O Units. *Inorg. Chem.* **56**, 6352-6361 (2017).
37. G. Qiu, R. R. Knowles, Rate–Driving Force Relationships in the Multisite Proton-Coupled Electron Transfer Activation of Ketones. *J. Am. Chem. Soc.* **141**, 2721-2730 (2019).
38. C. Riplinger, M. D. Sampson, A. M. Ritzmann, C. P. Kubiak, E. A. Carter, Mechanistic Contrasts between Manganese and Rhenium Bipyridine Electrocatalysts for the Reduction of Carbon Dioxide. *J. Am. Chem. Soc.* **136**, 16285-16298 (2014).
39. P. T. Smith, S. Weng, C. J. Chang, An NADH-Inspired Redox Mediator Strategy to Promote Second-Sphere Electron and Proton Transfer for Cooperative Electrochemical CO_2 Reduction Catalyzed by Iron Porphyrin. *Inorg. Chem.* **59**, 9270-9278 (2020).

Acknowledgments: We thank Liam Grunwald and Ahmed Mouchfiq for technical assistance and preliminary studies and Dr René Verel for assistance with NMR studies.

Funding:

Agence Nationale pour la Recherche, ANR Jeune Chercheur-Jeune Chercheuse ANR-17-CE05-0021 (SD, VM)

European Research Council (ERC) under the European Union's Horizon 2020 research and innovation programme (grant agreement No. [853064]) (SD, FM, VM)

Swiss National Science Foundation (SNSF) project funding (grant No 200021_197153 / 1 (VM))

Author contributions:

Conceptualization: SD, VM

Methodology: SD, VM

Investigation: SD, FM, EB

Funding acquisition: VM

Project administration: MF, VM

Supervision: VM

Writing – original draft: SD, FM, VM

Writing – review & editing: SD, FM, MF, VM

Competing interests: Authors declare that they have no competing interests.

Data and materials availability: All data are available in the main text or the supplementary materials.